

A MURINE *STAPHYLOCOCCUS AUREUS* FRACTURE-RELATED INFECTION MODEL CHARACTERISED BY FRACTURE NON-UNION, STAPHYLOCOCCAL ABSCESS COMMUNITIES AND MYELOID-DERIVED SUPPRESSOR CELLS

M.I. Hofstee^{1,2}, M. Riool², F. Gieling¹, V. Stenger¹, C. Constant¹, D. Nehrbass¹, S. Zeiter¹, R.G. Richards¹, S.A.J. Zaat² and T.F. Moriarty^{1,*}

¹AO Research Institute Davos, Davos Platz, Switzerland

²Amsterdam UMC, University of Amsterdam, Department of Medical Microbiology and Infection Prevention, Amsterdam Institute for Infection and Immunity, Amsterdam, the Netherlands

Abstract

A fracture-related infection (FRI) is a serious complication that can occur after surgical fixation of bone fractures. Affected patients may encounter delayed healing and functional limitations. Although it is well established that *Staphylococcus aureus* (*S. aureus*) is the main causative pathogen of an FRI, the pathophysiology of an *S. aureus*-induced FRI is not well characterised over time. Therefore, an experimental study in mice comparing *S. aureus*-inoculated and non-inoculated groups was performed that particularly focused on staphylococcal abscess communities (SACs) and host cellular response.

C57Bl/6N female mice received a double osteotomy of the femur, which was stabilised using a titanium 6-hole MouseFix locking plate and four screws. Animals were either *S. aureus*-inoculated or non-inoculated and euthanised between 1 and 28 d post-surgery. Histopathological evaluation showed normal bone healing for non-inoculated mice, whereas inoculated mice had no fracture consolidation and severe osteolysis. Within the bone marrow of inoculated mice, SACs were observed from 7 d, which increased in size and number over time. A fibrin pseudocapsule enclosed the SACs, which were surrounded by many Ly6G⁺ neutrophils with some Ly6C⁺ monocytes and F4/80⁺ macrophages, the majority of which were viable. The abscesses were encapsulated by fibrin(ogen), collagen and myofibroblasts, with regulatory T cells and M2 macrophages at the periphery. Only bone marrow monocytes and neutrophils of inoculated mice displayed functional suppression of T cells, indicative of myeloid-derived suppressor cells.

The present study revealed that an FRI in mice is persistent over time and associated with osteolysis, SAC formation and an immunosuppressive environment.

Keywords: *Staphylococcus aureus*, fracture-related infection, staphylococcal abscess community, myeloid-derived suppressor cell, immunosuppression.

***Address for correspondence:** Thomas Fintan Moriarty, PhD, AO Research Institute Davos, Clavadelerstrasse 8, 7270 Davos, Switzerland.

Telephone number: +41 814142397 E-mail: fintan.moriarty@aofoundation.org

Copyright policy: This article is distributed in accordance with Creative Commons Attribution Licence (<http://creativecommons.org/licenses/by-sa/4.0/>).

List of Abbreviations

AAALAC	Association for Assessment and Accreditation for Laboratory Animal Care	ClfA	clumping factor A
ANOVA	analysis of variance	Coa	coagulase
APC	allophycocyanin	DAPI	4',6-diamidino-2-phenylindole
Arg-1	arginase-1	Eap	extracellular adherence protein
BB	Brown and Brenn	EDTA	ethylenediaminetetraacetic acid
CCOS	culture collection of Switzerland	Emp	extracellular matrix protein
CD	cluster of differentiation	FACS	fluorescence-activated cell sorting
CFU	colony forming unit	FBS	foetal bovine serum
		FITC	fluorescein isothiocyanate
		FOXP3	forkhead box P3
		FRI	fracture-related infection
		G&E	giemsa and eosin

HBSS	Hank's buffered salt solution
H&E	haematoxylin and eosin
HOES	histopathological osteomyelitis evaluation score
IL	interleukin
iNOS	inducible nitric oxide synthase
Ly6	lymphocyte antigen 6
MDSC	myeloid-derived suppressor cell
MMA	methyl methacrylate
NO	nitric oxide
PBS	phosphate-buffered saline
PBS-T	PBS Tween 20
PE	phycoerythrin
PGE2	prostaglandin E2
PJI	prosthetic joint infection
PMN	polymorphonuclear cell
rIL-2	recombinant IL-2
ROS	reactive oxygen species
RPMI	Roswell Park Memorial Institute
RT	room temperature
<i>S. aureus</i>	<i>Staphylococcus aureus</i>
SAC	staphylococcal abscess community
SPF	specific-pathogen free
TGF- β	transforming growth factor beta
TLR	toll-like receptor
Treg	regulatory T cell
TSB	tryptic soy broth
TUNEL	terminal deoxynucleotidyl transferase dUTP nick end labelling
vWbp	von Willebrand factor-binding protein
α SMA	alpha smooth muscle actin

Introduction

FRI is one of the most serious complications associated with the surgical fixation of bone fractures. The rate of FRI in closed fractures ranges between 1-2 %, whereas it can reach up to 30 % for open fractures (Trampuz and Zimmerli, 2006). *S. aureus* is the predominant causative pathogen in an FRI, causing approximately 30 % of cases (Trampuz and Zimmerli, 2006). Unfortunately, treatment efforts fail in 4 to 11 % of cases, leading to further surgical revisions, lifelong suppression therapy or even amputation of the affected limb (Bezstarosti *et al.*, 2019; Bose *et al.*, 2015; Huh *et al.*, 2011; Kanakaris *et al.*, 2014). When specifically examining failure rates for FRI patients treated with implant retention, recurrence of infection varied from 0 to 14 % for patients that had a revision surgery within 3 weeks of infection, 11 to 18 % for patients that had a revision surgery within 3-10 weeks of infection and 33 % for patients that had a revision surgery after 10 weeks of infection (Morgenstern *et al.*, 2021). Although early revision surgery does reduce the risk of recurrent infection, current treatment efforts are not ideal and may need to be combined with different strategies.

Traditionally, an FRI has been classified as acute or chronic based upon time elapsed from initial

surgery and symptom onset (Metsemakers *et al.*, 2016). The distinction between acute and chronic FRI is also linked to the pathophysiology and treatment, however, this transition is poorly described in the literature and a clear time-related cut-off has never been scientifically defined (Morgenstern *et al.*, 2021). In the early stages of an acute FRI, the infiltrating immune cells are predominantly PMNs, whilst in a chronic FRI, the local inflammatory cells are predominantly macrophages (Klosterhalfen *et al.*, 1996). A chronic FRI is also associated with osteolysis, sequestrum formation and non-union (Alt *et al.*, 2011; Metsemakers *et al.*, 2016; Ochsner and Hailemariam, 2006).

One recently described feature of the pathophysiology of *S. aureus* infection is the SAC, which has been identified in the renal and peritoneal tissue (Cheng *et al.*, 2009; Cheng *et al.*, 2010; Rauch *et al.*, 2012) and in the bone marrow (Brandt *et al.*, 2018; Farnsworth *et al.*, 2017). SACs form the centre of abscesses and are surrounded by an amorphous pseudocapsule comprised of fibrin deposits (Cheng *et al.*, 2011; Cheng *et al.*, 2010; Thomer *et al.*, 2016b) formed by the action of the *S. aureus*-produced enzymes Coa and vWbp (Bjerketorp *et al.*, 2004; Friedrich *et al.*, 2003; Thomer *et al.*, 2016b). This pseudocapsule appears to serve as a barrier to invasion of immune cells, causing them to accumulate in large numbers at the periphery, leading to the persistence of *S. aureus* (Brandt *et al.*, 2018; Cheng *et al.*, 2010; Hofstee *et al.*, 2020a; Kobayashi *et al.*, 2015; Thomer *et al.*, 2016b).

Persistence of *S. aureus* has also been linked to MDSCs, which can inhibit proinflammatory responses of monocytes/macrophages, and has been mainly studied in mice (Heim *et al.*, 2015a; Heim *et al.*, 2018; Heim *et al.*, 2015b; Heim *et al.*, 2014; Peng *et al.*, 2017). In mice, monocytic MDSCs are CD11b⁺ Ly6C^{high} Ly6G⁻, whereas granulocytic MDSCs are CD11b⁺ Ly6C^{low} Ly6G⁺. Regular murine monocytes and neutrophils have the same phenotypical markers as monocytic and granulocytic MDSCs, which makes identifying murine MDSCs with immunohistochemical stains challenging. What sets monocytic and granulocytic MDSCs aside from regular monocytes and neutrophils are their immunosuppressive abilities, which are facilitated by the enzymes iNOS and/or Arg-1 (Ostrand-Rosenberg and Fenselau, 2018; Veglia *et al.*, 2018) and usually proven in functional T cell suppression assays (Bronte *et al.*, 2016). For *S. aureus* infections, whether MDSCs are distributed amongst the bone marrow or arranged in an organised manner is unknown.

The aim of the present study was to examine SAC formation in a murine FRI model and investigate whether MDSCs were present within bone marrow of these mice and possibly associated with SACs and/or abscess structures. Furthermore, the aim was to identify the host macromolecules associated with SAC formation, including fibrinogen and collagen. A femoral double osteotomy mouse model was

used where a femoral bone segment was created, which was either not inoculated or inoculated with *S. aureus*, and the femur was stabilised using a titanium 6-hole MouseFix locking plate. Immuno(fluorescent) stainings, HOES (Tiemann *et al.*, 2014) and *ex vivo* analyses were performed to investigate differences between inoculated and non-inoculated mice, with a particular focus on the maturation of SACs over time and possible immunosuppressive properties of the involved host cells.

Materials and Methods

Animals

All animal experiments were approved by the ethical committee of the Canton of Graubünden, Switzerland (approval number 2017_28 and 2019_10) and were carried out in an AALAC International accredited facility. 74 SPF C57Bl/6N female mice (Charles River) 20-28 weeks old at the time of surgery were used. Animals were acclimatised for at least 2 weeks prior to surgical intervention. Mice were divided randomly into *S. aureus*-inoculated and non-inoculated groups. Time points for sacrifice were 1, 3, 7, 14, 21 and 28 d post-surgery ($n = 6$ per subgroup) for inoculated mice and 3, 14 and 28 d ($n = 6$ per subgroup) for non-inoculated animals used for histological outcome parameters. Mice used for CFU quantification and *ex vivo* cultures were sacrificed 21 d post-surgery for both the inoculated group ($n = 6$) and non-inoculated group ($n = 6$). Cages were randomly assigned to the different subgroups. Individual ventilated cages (Techniplast, Schwerzenbach, Switzerland and Allentown, Schlieren, Switzerland) housed 2 to 6 mice each, were under 12 h light/dark cycle and were enriched with a plastic house, paper as well as wood for gnawing. Both water and food (3436, Provimi Kliba AG, Kaiseraugst, Switzerland) were provided *ad libitum*.

Bacteria and inoculum preparation

S. aureus JAR 06.01.31 (CCOS number 890, Wädenswil, Switzerland), obtained from a patient with an orthopaedic device-related infection (Moriarty *et al.*, 2010), was used for inoculum preparation. An overnight culture was prepared the day before surgery by incubating one colony in 50 mL TSB (Oxoid, Basel, Switzerland) at 37 °C while shaking. From the overnight culture, a fresh logarithmic phase culture was prepared in TSB. Bacteria were washed twice with PBS (Gibco) 1.5 h before surgery and diluted in PBS to obtain a 1 μ L inoculum containing approximately 1×10^4 CFU. 1 μ L sterile PBS was used as control.

Surgery and animal welfare

Prior to surgery, animals were anaesthetised by induction with sevoflurane (~ 5 % in O₂, flow rate 1 L/min; Sevofluran Baxter, Baxter AG). During surgery, the anaesthesia was maintained using

sevoflurane (~ 2-3 % in O₂, flow rate 0.6-1 L/min). Intraoperative analgesia consisted of buprenorphine (0.1 mg/kg subcutaneously; Bupaq, Streuli Pharma AG, Uznach, Switzerland) and carprofen (5 mg/kg subcutaneously; Norocarp, unfamed AG, Sursee, Switzerland) injected immediately after anaesthetic induction. After clipping and aseptically preparing the surgical field, a skin incision was made from the tail base to the left stifle. The subcutaneous fascia lata was cut and the level between the quadriceps and biceps femoris muscle was bluntly dissected. The left femur was stabilised with a titanium 6-hole MouseFix locking plate (RISystems AG, Davos Platz, Switzerland) and 4-outermost screws were inserted. The 2-inner screw-holes were left empty and used to generate 2 osteotomies with the MouseFix Drill&Saw guide (RISystems) and a Gigly hand saw (RISystems, 0.22 mm diameter). This created a 2 mm femoral segment. This segment was taken out and 1 μ L of either bacterial inoculum or sterile PBS was pipetted on top of the bone marrow of the segment. The inoculum or saline could absorb into the bone for 3 min before the segment was placed back into its original place without fixation. The fascia lata and the skin were closed with continuous sutures (5-0 Vicryl rapide, Ethicon, Courcelles, Belgium). Post-operative analgesia consisted of buprenorphine (0.1 mg/kg subcutaneously) every 4-10 h for 24 h as well as paracetamol (1.9 mg/mL) added to the drinking water for 7 d (DAFALGAN sirup for children, Bristol-Myers Squibb SA, Steinhausen, Switzerland). Post-operative radiographs were taken to confirm that the osteotomy and plate position were correct and to check for fractures. The mice wellbeing was checked daily by an animal caretaker and scored twice a day until 5 d post-surgery, followed by daily scoring up to 7 d and twice per week thereafter. Animals were monitored for their general and eating behaviour and the load they placed on the operated leg. External appearance and wound status were also monitored. Weight was monitored 3 and 7 d post-surgery and weekly thereafter. Mice were sacrificed by inducing general anaesthesia with sevoflurane followed by cervical dislocation.

Fixation, sectioning and stains

Some of the left femoral bones ($n = 24$) were fixed in 70 % methanol immediately after euthanasia. The fixed samples were embedded in MMA (Sigma-Aldrich) with the implant left in place. Sections (200 μ m) were prepared using a Leica 1600 rotating saw microtome (Leica microsystems), rehydrated with 1-acetoxy-2-methoxyethane and ethanol gradient and stained with 15 % (v/v) giemsa and 1 % (v/v) eosin (G&E; both Sigma-Aldrich). Images were taken with an Olympus BX63 brightfield microscope (Olympus).

For paraffin-wax-embedded samples ($n = 26$), left femora were fixed with formalin and subsequently decalcified using 12.5 % (w/v) EDTA (Roth AG) and 1.25 % (w/v) sodium hydroxide (Sigma-Aldrich)

decalcification solution. Then, implants were removed and the remaining bone and soft tissue was embedded in paraffin wax (Leica microsystems). Paraffin wax sections (5 μm) were cut using a paraffin wax HM 355 S microtome (Microm, Thermo Fisher Scientific), dewaxed and rehydrated through a descending ethanol gradient. Sections were either stained with Mayer's haematoxylin and 1 % (v/v) eosin (H&E; both Sigma-Aldrich), BB (Brown and Brenn, 1931), TUNEL assay to detect apoptotic cells (Abcam; #ab206386, manufacturer's protocol was used), picro-Mallory, picro-sirius red or immuno(fluorescent) stains. For more details on the last three stains, see below.

Picro-Mallory trichrome stain

To allow the acid dyes to stain more intensely, sections were post-fixed with Bouin's fluid [9 % (v/v) formaldehyde and 5 % (v/v) acetic acid in water-saturated picric acid 0.9 % (v/v)] overnight at RT. Then, sections were rinsed in distilled water to remove the Bouin's fluid. Weigert's iron haematoxylin (Sigma-Aldrich), prepared following the manufacturer's instructions, was applied for 20 min to stain nuclei and samples were stained with a picro-Mallory trichrome staining following a previously described protocol (Lendrum *et al.*, 1962).

Picro-sirius red stain

Sections were stained with Weigert's iron haematoxylin for 8 min and differentiated in lukewarm running tap water. Then, sections were placed into the picro-sirius red solution [0.1 % (w/v) sirius red F3B (Sigma-Aldrich) in water-saturated picric acid] for 1 h. Samples were washed twice using 1 % (v/v) aqueous acidified acid and most of the water was removed by shaking the sections.

Immuno(fluorescent) stains

An antigen retrieval step was performed by boiling the sections in sodium citrate buffer (0.1 mol/L, pH 6.0; Sigma-Aldrich) for 15 min. Endogenous peroxidase was blocked by incubation for 30 min in methanol containing hydrogen peroxide [0.3 % (v/v) H_2O_2 in absolute methanol] for samples subsequently stained with a peroxidase-linked antibody. Samples stained with fluorescently labelled secondary antibodies were incubated for 5 min in absolute methanol. Sections were washed twice in PBS with 0.1 % (v/v) Tween 20 (PBS-T; both Sigma-Aldrich) and blocked by incubation with 5 % (v/v) animal-free blocker (Vector Laboratories, Burlingame, CA, USA) in PBS-T for 1 h at RT in a moist chamber. Blocking buffer was removed and sections were incubated overnight at 4 °C with primary antibodies in PBS-T with 0.5 % (v/v) animal-free blocker. Primary antibodies were omitted for negative control sections. See Table 1 for the different primary antibody combinations, concentrations, targets and matching secondary antibodies. Secondary antibodies were applied after overnight incubation with the primary antibodies.

Samples were washed three times with PBS-T before each incubation step. All secondary antibodies were diluted 1 : 200 in PBS-T with 0.5 % (v/v) animal-free blocker and were incubated for 30 min at RT in the dark. Lastly, sections were incubated with Trueview and coverslipped using Vectashield vibrance antifading mounting medium with DAPI (both Vector Laboratories) according to manufacturer's instructions (Table 1; staining 1-7). Alternatively, samples were incubated with ABC complex and ImmPACT DAB solution (both Vector Laboratories) following the manufacturer's instructions and counterstained with Mayer's haematoxylin (Table 1; staining 8).

Non-fluorescently stained paraffin wax samples were mounted using Eukitt mounting medium (Sigma-Aldrich) and imaged using an Olympus BX63 microscope. Immunofluorescently-stained samples were examined using a Zeiss LSM 800 inverse fluorescence microscope and image processing was performed using the ZEN (blue edition) software (Zeiss).

Histopathological osteomyelitis evaluation score

G&E-stained MMA-embedded femora ($n = 2$ or 3) with an inoculated or non-inoculated bone segment were evaluated by a pathologist using the HOES (Tiemann *et al.*, 2014). This score evaluates three acute osteomyelitis features (A1-3) and two chronic osteomyelitis features (C1-2). Osseonecrosis (A1), soft tissue necrosis (A2) and granulocyte infiltration (A3) were scored as indicators of acute osteomyelitis, whereas bone neogenesis/fibrosis (C1) and lymphocyte/macrophage infiltration (C2) were evaluated as features of chronic osteomyelitis. The 5 above mentioned parameters were scored from 0 to 5 (Table 2).

SAC size

Images of SACs in paraffin-wax- or MMA-embedded samples were taken using the Zeiss Axio Vert.A1 microscope (Zeiss). SAC number was determined for one section per mice and SAC size was established by measuring horizontal and vertical length of SACs with the measuring tool from the AxioVision SE64 software (Zeiss) and calculating the surface area (in mm^2) of the SACs.

Bone marrow cell sorting

Soft tissue and implants were removed from the operated femora of inoculated ($n = 5$) and non-inoculated mice ($n = 5$) and used for CFU quantification. The outer ends of the femoral bones were cut off and bone marrow cells were flushed out using a 24G \times 1 needle attached to a 2 mL syringe containing HBSS (Gibco). The collected cells were passed through a 70 μm cell strainer and centrifuged at 300 \times g for 6 min at 4 °C. Bone marrow supernatant was collected for CFU quantification and the cell pellet was incubated with 5 mL red blood cell lysis buffer [15 mmol/L NH_4Cl , 1 $\mu\text{mol/L}$ KHCO_3 (both

Table 1. Different primary antibody combinations with the dilutions used per antibody and their corresponding secondary antibody mixtures.

Stain	Target	Primary antibodies	Dilutions	Secondary antibodies Incubation 1	Secondary antibodies Incubation 2	Secondary antibodies Incubation 3
1	1) Neutrophils 2) Fibrin(ogen) 3) Macrophages	1) Rat monoclonal anti-Ly6G antibody (BD Bioscience, 551459) 2) Rabbit polyclonal affinity purified anti-fibrinogen antibody (Innovative Research, IASMFBN-GF-HT) 3) Chicken polyclonal anti-F4/80 antibody (Abcam, ab186073)	1) 1 : 100 2) 1 : 100 3) 1 : 50	3) Goat anti-chicken IgY (Abcam, ab175755)	3) Donkey anti-goat IgG Alexa Fluor Plus 647 (Thermo Fisher Scientific, A32849)	1) Goat anti-rabbit IgG Alexa Fluor 568 (Thermo Fisher Scientific, A-11036) 2) Goat anti-rat IgG Alexa Fluor 488 (Thermo Fisher Scientific, A-11006)
2	1) Fibrin(ogen) 2) Myofibroblasts	1) Rabbit polyclonal affinity purified anti-fibrinogen antibody 2) Goat polyclonal anti-alpha smooth muscle actin antibody (Abcam, ab21027)	1) 1 : 100 2) 1 : 200	2) Donkey anti-goat IgG Alexa Fluor Plus 647	1) Goat anti-rabbit IgG Alexa Fluor 568	
3	1) <i>Staphylococcus aureus</i> 2) Neutrophils 3) Macrophages	1) Rabbit polyclonal anti- <i>Staphylococcus aureus</i> antibody (Abcam, ab20920) 2) Rat monoclonal anti-Ly6G antibody 3) Chicken polyclonal anti-F4/80 antibody	1) 1 : 500 2) 1 : 100 3) 1 : 50	3) Goat anti-chicken IgY	3) Donkey anti-goat IgG Alexa Fluor Plus 647	1) Goat anti-rabbit IgG Alexa Fluor 568 2) Goat anti-rat IgG Alexa Fluor 488
4	1) Monocytes 2) Pan-myeloid cells	1) Rat monoclonal anti-Ly-6C antibody (Biolegend, 128002) 2) Rabbit monoclonal anti-CD11b (Abcam, ab133357)	1) 1 : 20 2) 1 : 500	1) Goat anti-rat IgG Alexa Fluor 488 2) Goat anti-rabbit IgG Alexa Fluor 568		
5	1) Neutrophils 2) Enzyme NO production 3) Enzyme urea cycle	1) Rat monoclonal anti-Ly6G antibody 2) Rabbit polyclonal anti-iNOS antibody (Abcam, ab15323) 3) Goat polyclonal anti-arginase 1 antibody (Genetex, GTX88484)	1) 1 : 50 2) 1 : 50 3) 1 : 200	3) Donkey anti-goat IgG Alexa Fluor Plus 647	1) Goat anti-rat IgG Alexa Fluor 488 2) Goat anti-rabbit IgG Alexa Fluor 568	
6	1) Monocytes 2) Enzyme NO production 3) Enzyme urea cycle	1) Rat monoclonal anti-Ly-6C antibody 2) Rabbit polyclonal anti-iNOS antibody 3) Goat polyclonal anti-arginase 1 antibody	1) 1 : 20 2) 1 : 50 3) 1 : 200	3) Donkey anti-goat IgG Alexa Fluor Plus 647	1) Goat anti-rat IgG Alexa Fluor 488 2) Goat anti-rabbit IgG Alexa Fluor 568	
7	1) Macrophages 2) Enzyme NO production 3) Enzyme urea cycle	1) Chicken polyclonal anti-F4/80 antibody 2) Rabbit polyclonal anti-iNOS antibody 3) Goat polyclonal anti-arginase 1 antibody	1) 1 : 50 2) 1 : 50 3) 1 : 200	3) Donkey anti-goat IgG Alexa Fluor Plus 647	1) Goat anti-chicken IgY Alexa Fluor 488 (Thermo Fisher Scientific, A-11039) 2) Goat anti-rabbit IgG Alexa Fluor 568	
8	1) Regulatory T cells	1) Rat monoclonal anti-FoxP3 antibody (Invitrogen, 14-5773-82)	1) 1 : 50	1) Biotinylated anti-rat IgG (Vector labs, BA9400)		

Table 2. Severity scores used to score the five different acute and chronic osteomyelitis markers of the HOES.

Severity score	Description
0	A feature was absent in the tissue
1	A feature was slightly noticeable within the tissue
2	A feature was focally present in the tissue
3	A feature was multi-focally present in the tissue
4	A feature was more than 50 % present in the tissue
5	The whole tissue was affected by a feature

Sigma-Aldrich) and 10 $\mu\text{mol/L}$ EDTA] for 5 min at RT. Next, 25 mL RPMI (Gibco) medium supplemented with 3 % (v/v) FBS (Sigma-Aldrich) was added and cells were centrifuged at 300 $\times g$ for 6 min at 4 °C. In preparation for the FACS staining, cells were washed using 10 mL of sorting buffer [HBSS with 0.5 % (w/v) bovine serum albumin (Sigma-Aldrich) and 2 mmol/L EDTA]. After centrifuging the suspension at 300 $\times g$ for 6 min at 4 °C and discarding the supernatant, cells were incubated with FC-receptor blocking reagent (BD Bioscience) for 10 min at 4 °C. Subsequently, antibody mixtures containing anti-CD11b-APC, anti Ly6G-FITC and anti Ly6C-PE (all Biolegend) were added to the samples and let to incubate for 30 min at 4 °C. Samples were washed twice with sorting buffer, resuspended in sorting buffer, passed through a 70 μm cell strainer and DAPI (Sigma-Aldrich) was added to stain dead cells. Sorting was performed using a BD FACSDiva (BD Bioscience) using a 100 μm nozzle and gating for CD11b⁺ Ly6C⁺ Ly6G⁻ and CD11b⁺ Ly6C⁺ Ly6G⁺ cell populations. Cells were sorted with an efficiency above 86 % and purified cells were kept on ice until further use.

T cell suppression assay

Splenocytes were isolated from spleens of non-inoculated mice by pushing the spleens through a 70 μm cell strainer placed on a 5 mL tube with the plunger of a 5 mL syringe. The cell strainer was washed with 5 mL RPMI containing 3 % FBS, the cell suspension was centrifuged at 300 $\times g$ for 6 min at 4 °C, supernatant was discarded and red blood cells within the cell pellet were lysed using 5 mL lysis buffer for 4 min at RT. After adding 25 mL RPMI containing 3 % FBS, cells were spun down at 300 $\times g$ for 6 min at 4 °C, washed with 10 mL RPMI containing 10 % (v/v) FBS, centrifuged at 300 $\times g$ for 6 min at 4 °C and resuspended in 20 mL RPMI containing 10 % FBS. The splenocyte suspension was filtered using a cell strainer and stained with the membrane dye PKH26 (1.2 μL per 1×10^7 splenocytes; Sigma-Aldrich) following manufacturer's instructions. Suppression of T cell proliferation was assessed by co-culturing 0.5×10^5 PKH26-stained splenocytes/96-well plate with previously sorted CD11b⁺ Ly6C⁺ Ly6G⁻ or CD11b⁺ Ly6C⁺ Ly6G⁺ bone marrow cells from inoculated or non-inoculated mice in RPMI supplemented with 10 % FBS, 1 % (v/v) penicillin/streptomycin (Sigma-Aldrich), 1 mmol/L sodium pyruvate (Sigma-Aldrich) and 50 $\mu\text{mol/L}$ β -mercaptoethanol (Roth). Splenocytes

were stimulated with murine CD3/CD28 Dynabeads (1 : 1 ratio with splenocytes; Thermo Fisher Scientific) and 30 U/mL murine rIL-2 (Peprotech). Cells from non-inoculated mice were co-cultured 1 : 1, whereas cells from inoculated mice were co-cultured 1 : 1 and 0.5 : 1 with PKH26-stained splenocytes. The co-cultures were incubated for 4 d at 37 °C and 5 % CO₂, after which T cell proliferation was assessed by flow cytometry using CD3-FITC, CD4-Alexa Fluor 700 and CD8 α -APC antibodies (all Biolegend) and DAPI to visualise dead cells. Proliferation was normalised to T cells stimulated with CD3/CD28 Dynabeads and rIL-2, which were set to 100 %. Flow cytometric data was analysed using the Kaluza Analysis software (Beckman Coulter Life Sciences).

CFU quantification

CFU were quantified for soft tissue, bone, bone marrow supernatant and implant. Soft tissue or femoral bones were placed into 10 mL PBS and homogenised mechanically using Omni Tissue Homogenizer and Hard Tissue Homogenizing tips, respectively (both Omni International, Kennesaw, GA, USA). Implants were sonicated at 40 kHz for 3 min in 5 mL of PBS in an ultrasonic bath (Bandelin Sonorex, Berlin, Germany). Serial dilutions were made from all 4 type of samples per mouse and 10 μL of these dilutions were plated in triplicate on 5 % horse blood agar plates (Oxoid). Plates were incubated at 37 °C and CFUs were determined after 24 and 48 h.

Data analysis

Data were analysed and visualised with GraphPad Prism 8 (GraphPad Software). Normality of data was checked using a Shapiro-Wilk test and by visually assessing QQ plots from the data. Parametric data was assessed using a Sidak multiple comparison test or a two-way ANOVA, whereas non-parametric data was examined using a Dunn's multiple comparison test. $p < 0.05$ was considered statistically significant.

Results

Clinical evaluation and animal welfare

Of the 74 operated mice, 60 were included in the final bacteriological and histological evaluation. 14 were operated but sacrificed before study completion and excluded from further analysis. 12 of these excluded

mice were sacrificed because of a fracture of the proximal femur, 1 animal had an open, draining wound at the surgical site and 1 was excluded for unstable fixation of the plate caused by screw loosening. The lost animals were not replaced. Upon study completion, all groups for histopathology had 6 mice per group, except for the inoculated groups evaluated after 7 and 21 d (both 5 mice) and 28 d (4 mice) due to losses described above. The animals operated for CFU quantification and *ex vivo* cell culture had 5 mice per group after losing 1 mouse per group.

Non-inoculated mice gained on average 2.5 % body weight after 28 d, while inoculated mice lost on average 6.5 % body weight (data not shown).

Radiographic and histopathological evaluation

The double femoral osteotomy model generated a 2 mm bone segment. At 3 d, non-inoculated mice did not show any signs of bone healing between the bone segment and the adjacent femoral bone (Fig. 1a-b). By 14 d, some early signs of healing were observed (Fig. 1c) with newly formed woven bone or soft

callus, characterised by an irregular, not condensed appearance of the bone (Fig. 1d; red arrow). Non-inoculated animals had complete healing of the femur revealed by complete bridging between the segment and adjacent bone after 28 d, although the newly formed bone was not yet compact (Fig. 1e-f). At this time, some osteoclasts were present and remodelling of the callus had commenced (Fig. 1f; black arrow). Bone marrow was observed within the newly formed bone (Fig. 1f; yellow arrow).

Inoculated animals displayed markedly different appearance, although at the earliest time point, 3 d, radiographic images were not significantly different from those of non-inoculated mice (Fig. 1g). At this time, the bone marrow contained small bacterial aggregates, without any marked infiltration of immune cells (Fig. 1h; arrowhead). By 14 d, there were no signs of bone healing (Fig. 1i) and the bacterial colonies were still present Fig. 1j; arrowhead). Early signs of osteolysis were revealed by the irregularly edged bone (Fig. 1j; black arrow). Some newly formed bone, which was not yet compact, was also present (Fig. 1j; red arrow). In contrast to non-inoculated

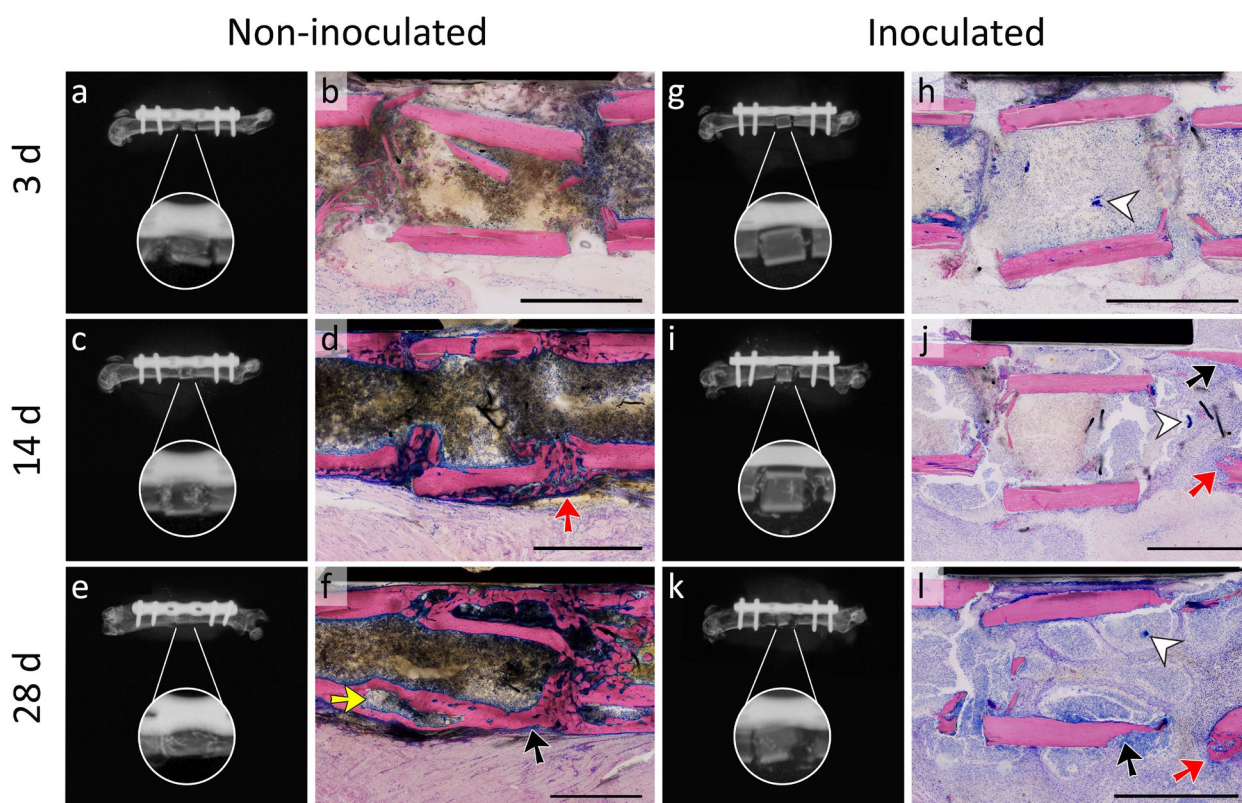


Fig. 1. Radiographic and histological appearance of non-inoculated and inoculated mice at 3, 14 and 28 d post-surgery. Representative radiographs and G&E-stained MMA-embedded sections of (a-f) non-inoculated or (g-l) *S. aureus*-inoculated mouse femoral bone at day 3 (upper row), 14 (middle row) and 28 (lower row) post-surgery. Mice received a double osteotomy within the femur, which created a bone segment, and a titanium 6-hole MouseFix locking plate for bone stabilisation. Non-inoculated animals showed signs of fracture consolidation, whereas inoculated mice still had a non-union 28 d post-surgery. G&E stained bone in pink and connective and soft tissue in purple, whereas nuclei are dark blue. Red arrows indicate bone regeneration, black arrows show bone resorption pits created by osteoclasts, white arrowheads point out bacterial aggregates and the yellow arrow indicate bone marrow within newly formed bone. Note, the samples of the non-inoculated mice stained more in brown within the bone marrow. This is an artifact due to incomplete dehydration and defatting. Black debris were remains of the Gigly wire used to make the double osteotomy. Scale bars: 1 mm.

mice, no fracture consolidation was visible in the inoculated animals after 28 d and their osteotomy ends were irregularly shaped, suggestive of osteolysis (Fig. 1k). Bacterial aggregates and remnants of osteoclast activity were detected (Fig. 1l; arrowhead and black arrow, respectively). Newly formed bone that was loosely arranged could also be observed in inoculated mice 28 d post-surgery (Fig. 1l; red arrow)

but this was minor compared to non-inoculated mice and severe bone osteolysis prevailed.

Additionally, samples of non-inoculated and inoculated mice were evaluated by scoring for bone-infection-related features using HOES (Tiemann *et al.*, 2014) (Fig. 2a) and immunostainings were performed to detect the presence of neutrophils, fibrin(ogen) and macrophages in the distal part of the bone segment

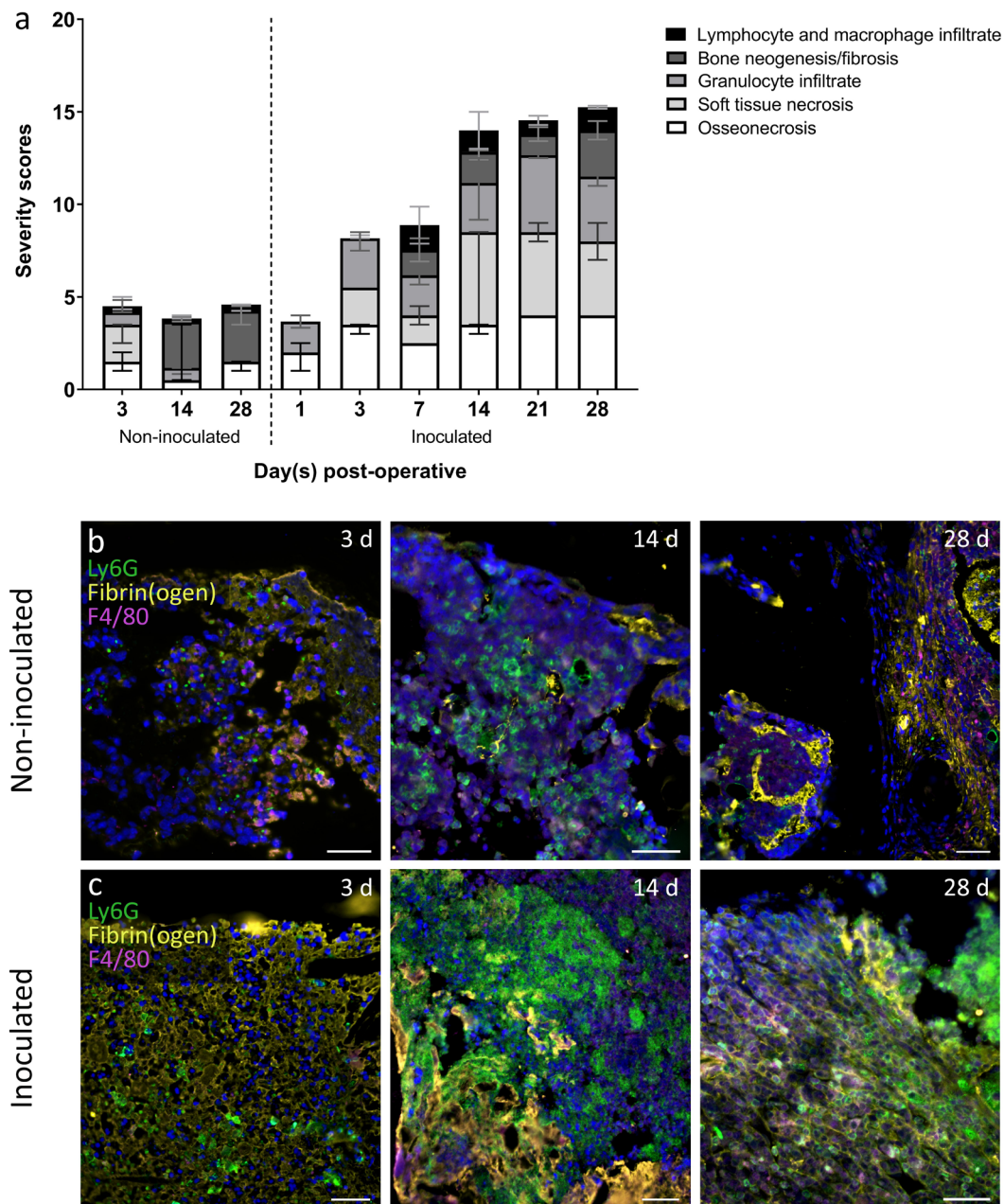


Fig. 2. Histopathological evaluation of non-inoculated and *S. aureus*-inoculated mice. (a) HOES of non-inoculated mice at 3, 14 and 28 d post-surgery and mice with a *S. aureus*-inoculated femoral bone segment assessed at 1, 3, 7, 14, 21 and 28 d post-infection. From bottom to top, the acute osteomyelitis features investigated were granulocyte infiltration (white), osseonecrosis (light grey) and soft tissue necrosis (medium grey); the chronic osteomyelitis features assessed were bone neogenesis/fibrosis (dark grey) and lymphocyte and macrophage infiltrate (black). Data shown are medians of HOES scores with 95 % confidence intervals from $n = 2$ for inoculated mice at 7 and 28 d post-surgery and $n = 3$ for the rest of the data. Representative images of host responses in paraffin-wax-embedded murine femoral bone of (b) non-inoculated and (c) *S. aureus*-inoculated mice at 3, 14 and 28 d post-surgery. For consistency, images were taken from the distal part of the bone segment of non-inoculated mice and inoculated mice. Immunofluorescent triple stains were performed for Ly6G (neutrophils, green), fibrin(ogen) (yellow) and F4/80 (macrophages, violet). DAPI (dark blue) was used as a nuclear counterstain. Scale bar: 50 μm .

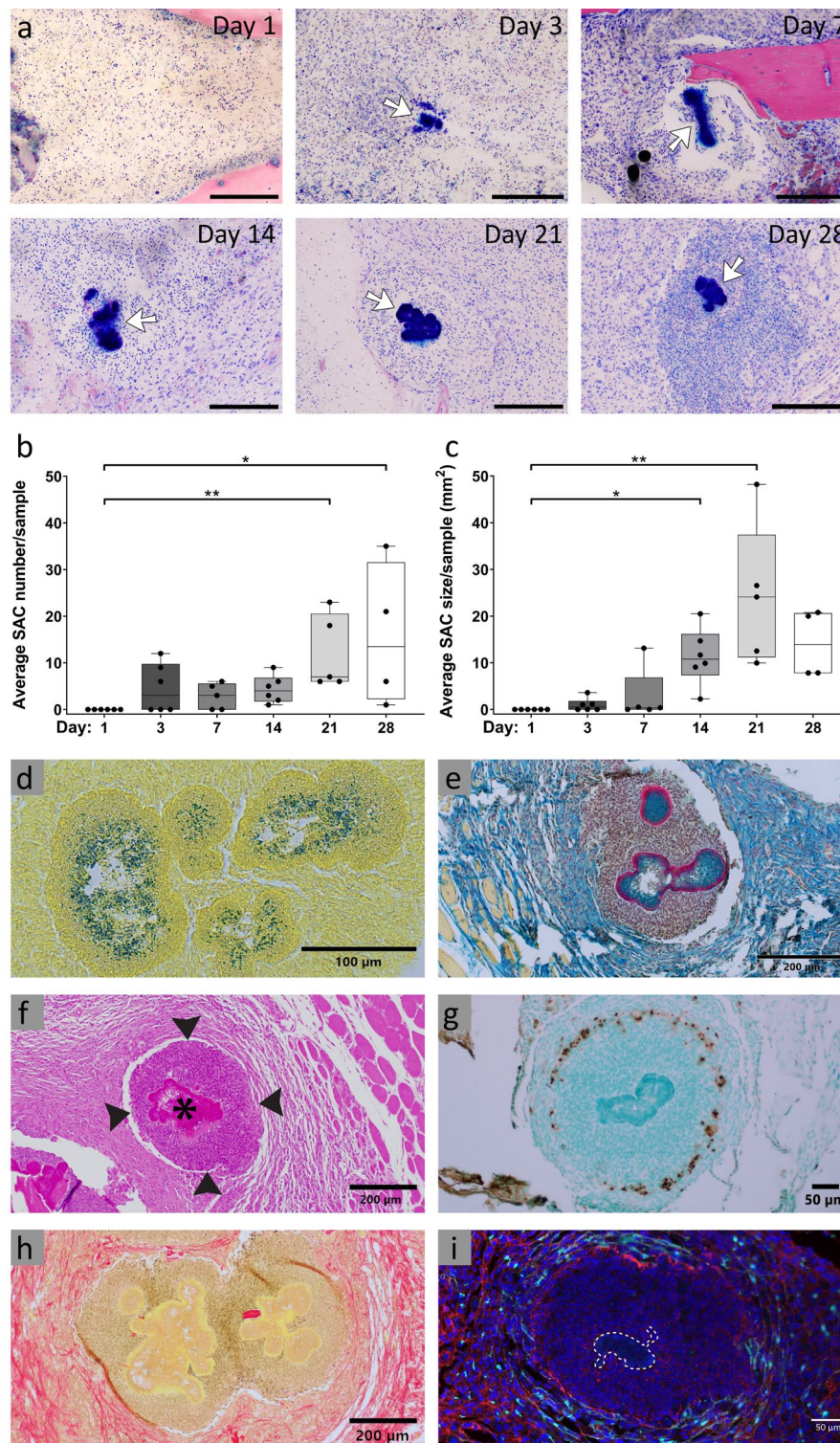


Fig. 3. Assessment of SACs and abscesses in femoral bone marrow of *S. aureus*-inoculated mice. (a) G&E-stained MMA-embedded femoral bone marrow of *S. aureus*-inoculated mice from 1, 3, 7, 14, 21 and 28 d post-surgery. Images are representative and focused on abscess structures with SACs, indicated with white arrows, present in the bone marrow. Scale bar: 200 μ m. SAC (b) number and (c) size measured in paraffin-wax- and MMA-embedded femoral bone marrow of *S. aureus*-inoculated mice 1, 3, 7, 14, 21 and 28 d post-surgery. Statistical test used: Dunn's multiple comparison test. Data are medians \pm max and min values of average SAC number and size per animal. $n = 6$ for 1, 3 and 14 d, $n = 5$ for 7 and 21 d and $n = 4$ for 28 d post-surgery. * $p < 0.05$, ** $p < 0.01$. Representative images of SACs in paraffin-wax-embedded murine femoral bone inoculated with *S. aureus* from 21 or 28 d stained with (d) BB for Gram⁺ bacteria (blue); (e) picro-Mallory trichrome for fibrin (magenta); (f) H&E, with a SAC indicated by an asterisk and host cells within an abscess by arrowheads; (g) TUNEL assay for apoptotic host cells, with methyl green as a counterstain (brown); (h) picro-Sirius for collagen fibres (red); (i) immunofluorescent antibodies for fibrin(ogen), α SMA for myofibroblasts, with DAPI as a nuclear counterstain and the SAC indicated by a dashed white line (red, turquoise and dark blue, respectively).

(Fig. 2b,c). Non-inoculated mice had a low degree of osseonecrosis at 3, 14 and 28 d. Soft tissue necrosis was only observed at 3 d, whereas granulocytes were present in bone and surrounding tissue at 3 and 14 d. A fibrin clot within the osteotomy gap was observed at 3 d, which evolved in fibrous tissue. Both the presence of fibrous tissue and bone neogenesis was noted from 14 d on, while lymphocytes and macrophages were present at all time points. Non-inoculated mice did not have acute osteomyelitis according to the HOES scoring system (*i.e.* the sum of osseonecrosis, soft tissue necrosis and granulocyte infiltrate scores was lower than 6).

In inoculated mice, from 1 to 28 d, osseonecrosis was observed in the bone segment and adjacent the femoral bone. The soft tissue above the implant became necrotic at 3 d and this increased at later time points. Large numbers of granulocytic cells were located within muscle and bone tissue at all time points together with many fibrin(ogen) fibres. Regeneration started from 7 d and continued until 28 d, indicated by bone neogenesis and fibrous tissue formation. Aside from granulocytes, from 7 d on, lymphocytes and macrophages also began infiltrating into bone and soft tissue from 7 d onwards. From 14 d, animals no longer had an acute infection but had transitioned to what is considered a chronically florid/active infection according to the HOES score (sum of all features was higher than 9). At later time points, mice had still not transitioned to a chronic infection since the sum score of bone neogenesis/fibrosis and lymphocyte and macrophage infiltration was lower than 6, granulocytes were still present even after 28 d of infection and only minor signs of bone regeneration were observed.

SACs

In inoculated animals, abscess structures were observed within bone marrow from 3 d onwards (Fig. 3a). In addition to the numerous abscesses observed, some biofilms on screws and implant were also present (data not shown). At the centre of the abscess, SACs were observed that appeared as dense blue-staining structures in G&E-stained sections (Fig. 3a, white arrows). From 14 d onwards, all inoculated animals had SACs, with significantly more SACs at 21 and 28 d compared to 1 d (Fig. 3b). SAC size significantly increased from 1 d to 14 and 21 d (Fig. 3c). Examination of a SAC and abscess in more detail showed that the centre of a SAC contained Gram⁺ bacteria (Fig. 3d; blue). These bacteria were covered with a pseudocapsule consisting of fibrin fibres (Fig. 3e; magenta). Around the SAC (Fig. 3f, asterisk) many leukocytes were present (Fig. 3f, arrowheads), which, together with the SAC, were mostly alive (Fig. 3g; green). Also, a rim of apoptotic cells was observed that did not border the SAC (Fig. 3g; brown). The SAC and its surrounding cells were encapsulated by layers of oriented but not consolidated collagen fibres (Fig. 3h; red) and fibrin(ogen) strands (Fig. 3i; red) and by α SMA⁺ myofibroblasts (Fig. 3i; turquoise). Together,

the SAC, adjacent immune cells and encapsulation formed the complete structure of what is named as abscess in the text below.

Immune cell infiltration towards SACs

To investigate which immune cells were associated with *S. aureus* aggregates/SACs present during acute or chronically florid infection, immunostainings with markers for different immune cells were performed at 7 and 21 d, respectively. Bone marrow after 7 d of infection (overview in Fig. 4a) contained a small number of *S. aureus* aggregates with few bacteria per aggregate together with some Ly6G⁺ neutrophils and F4/80⁺ macrophages (Fig. 4b). Successive sections showed that some Ly6C⁺ monocytes and CD11b⁺ myeloid cells were also dispersed around the same area of the *S. aureus* aggregates (Fig. 4c). At this time, no iNOS, Arg-1-expressing cells (Fig. 4d) or FOXP3⁺ Tregs were observed (Fig. 4e) neither organised structures were seen.

By 21 d, clearly defined abscess structures were observed in the bone marrow (Fig. 4f), with a central SAC staining positive for *S. aureus* (Fig. 4g; edge of the SAC is depicted). The SAC was surrounded by highly Ly6G⁺ neutrophils and a small number of F4/80⁺ macrophages at the border (Fig. 4g; white arrowheads). Some cells within the abscess were positive for the monocyte marker Ly6C and the leukocyte marker CD11b (Fig. 4h). iNOS⁺ and Arg-1⁺ cells at the border of the abscess formed into somewhat organised arrangements within the abscess (Fig. 4i; white arrows). FOXP3⁺ Tregs cells were present outside the abscess (Fig. 4j).

To further probe the cell populations within the abscess after 21 d of infection, and particularly to investigate neutrophil, monocyte and macrophage cell surface markers as well as the enzymes iNOS and Arg-1 used by macrophages but also MDSCs, further high magnification images were taken (Fig. 5). Fig. 5a-b shows the Ly6G neutrophil marker in combination with iNOS and Arg-1. The neutrophils (Ly6G) in close proximity to the SAC at the centre of the abscess expressed Arg-1 but not iNOS (Fig. 5a and b). H&E staining of the same section confirmed these locations contained neutrophils with either banded or partially segmented nuclei (Fig. 5c; white arrows). These neutrophils appeared intact and alive.

Co-localisation of iNOS and Arg-1 with Ly6C, a monocyte marker, is shown in Fig. 5d,e. Highly Ly6C⁺ cells were observed at the border of the abscess where the staining co-localised with both iNOS and Arg-1 staining (Fig. 5d,e). Such iNOS⁺ and Arg-1⁺ monocytic cells were not present at the centre of the abscess, near the SAC. H&E staining showed cells with morphological characteristics of monocytes, in the same areas at the edge of the abscess where the Ly6C⁺, iNOS⁺ and Arg-1⁺ cells were located (Fig. 5f; black arrows).

Co-localisation of iNOS and Arg-1 with F4/80, a macrophage marker, is shown in Fig. 5g,h. Few F4/80⁺ macrophages were observed, but those present were

generally seen at the periphery of the abscess and were strongly Arg-1⁺ and expressed iNOS to a lesser extent (Fig. 5g,h), indicative of an anti-inflammatory, M2 phenotype. The H&E staining also confirmed the presence of macrophages at this location (Fig. 5i; white arrowhead). F4/80- and Arg-1-expressing M2 macrophages were observed outside of the abscess as well.

T cell suppression by CD11b⁺ Ly6C⁺ Ly6G⁻ or CD11b⁺ Ly6C⁺ Ly6G⁺ bone marrow cells

To assess whether monocytes and/or neutrophils from non-inoculated or inoculated mice had immune suppressive capabilities, CD11b⁺ Ly6C⁺ Ly6G⁻ monocytes or CD11b⁺ Ly6C⁺ Ly6G⁺ neutrophils were purified from non-inoculated bone marrow or

bone marrow with many abscesses and SACs. CFU quantifications showed that non-inoculated mice did not have any detectable viable bacteria within soft tissue, bone and bone marrow samples or on implants after 21 d (Fig. 6a). In contrast, the samples from inoculated mice contained larger numbers of bacteria varying from 5 to 6.5 Log₁₀ total CFU, demonstrating that the inoculated animals were indeed infected after 21 d.

There was a significant difference in the percentage of monocytic CD11b⁺ Ly6C⁺ Ly6G⁻ cells and neutrophilic CD11b⁺ Ly6C⁺ Ly6G⁺ cells from the total bone marrow cell population between inoculated mice and non-inoculated mice (Fig. 6b).

A T cell suppression assay was performed with the purified monocytic CD11b⁺ Ly6C⁺ Ly6G⁻ cells

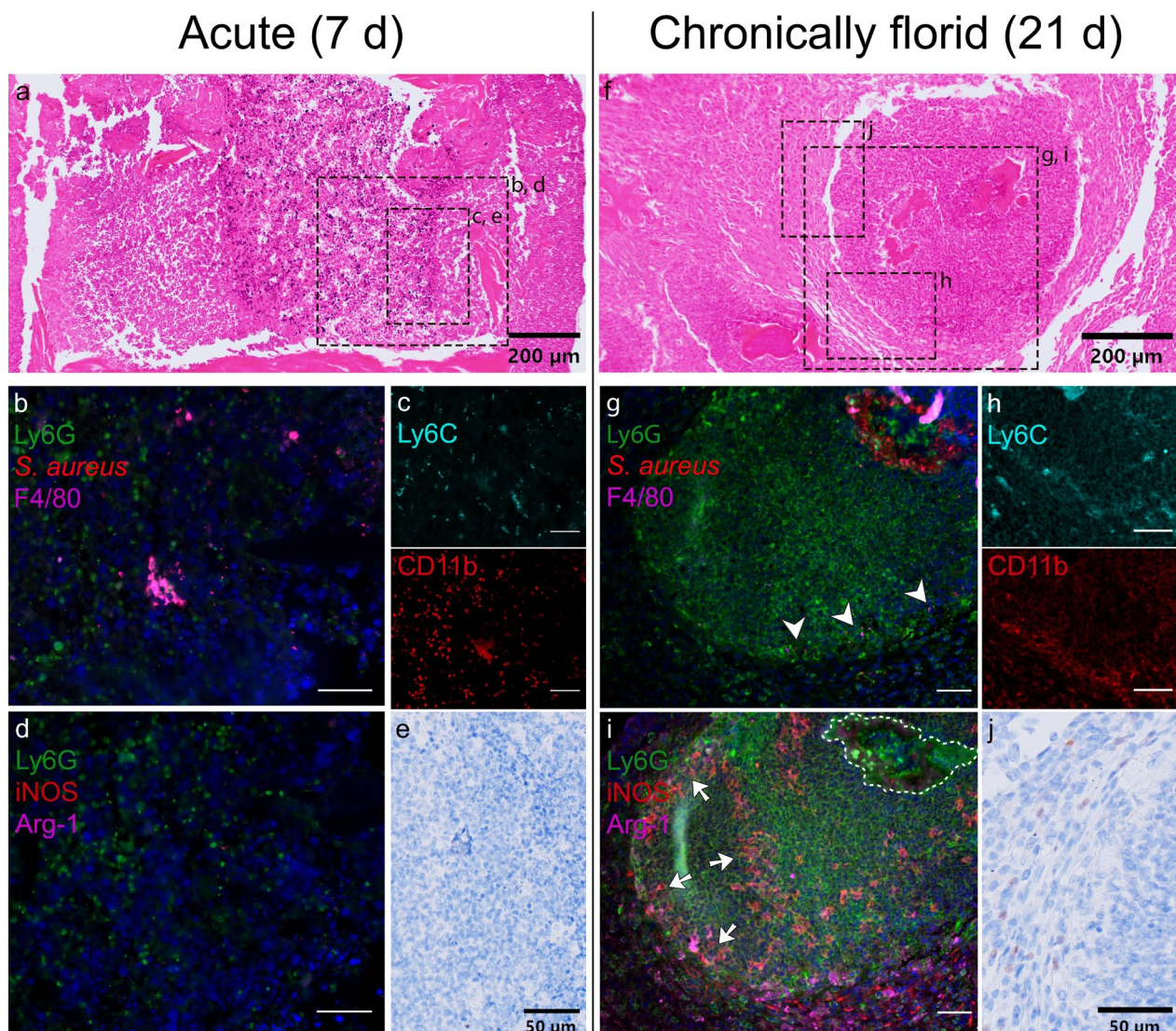


Fig. 4. Host cells associated with *S. aureus* aggregates in paraffin wax sections of inoculated mice 7 and 21 d post-surgery. (a) H&E, (b-d) immunofluorescent and (e) immunostaining of bone marrow within the *S. aureus*-infected segment after 7 d. (f) H&E, (g-i) immunofluorescent and (j) immunostaining of bone marrow with an abscess containing SACs after 21 d. Successive sections were used for *S. aureus* (red), Ly6G (neutrophils, green), F4/80 (macrophages, violet, white arrowheads), Ly6C (monocytic cells, turquoise), CD11b (pan-myeloid cells, red), iNOS (enzyme NO production, red), Arg-1 (enzyme urea cycle, violet), DAPI (nuclei, dark blue) and FOXP3 (brown) to visualise Tregs. Rim of cells positive for iNOS and Arg-1 are indicated by white arrows and co-localisation of Ly6G, F4/80 and *S. aureus* signals shown as a light pink colour. Scale bar: (b-d and g-i) 50 µm.

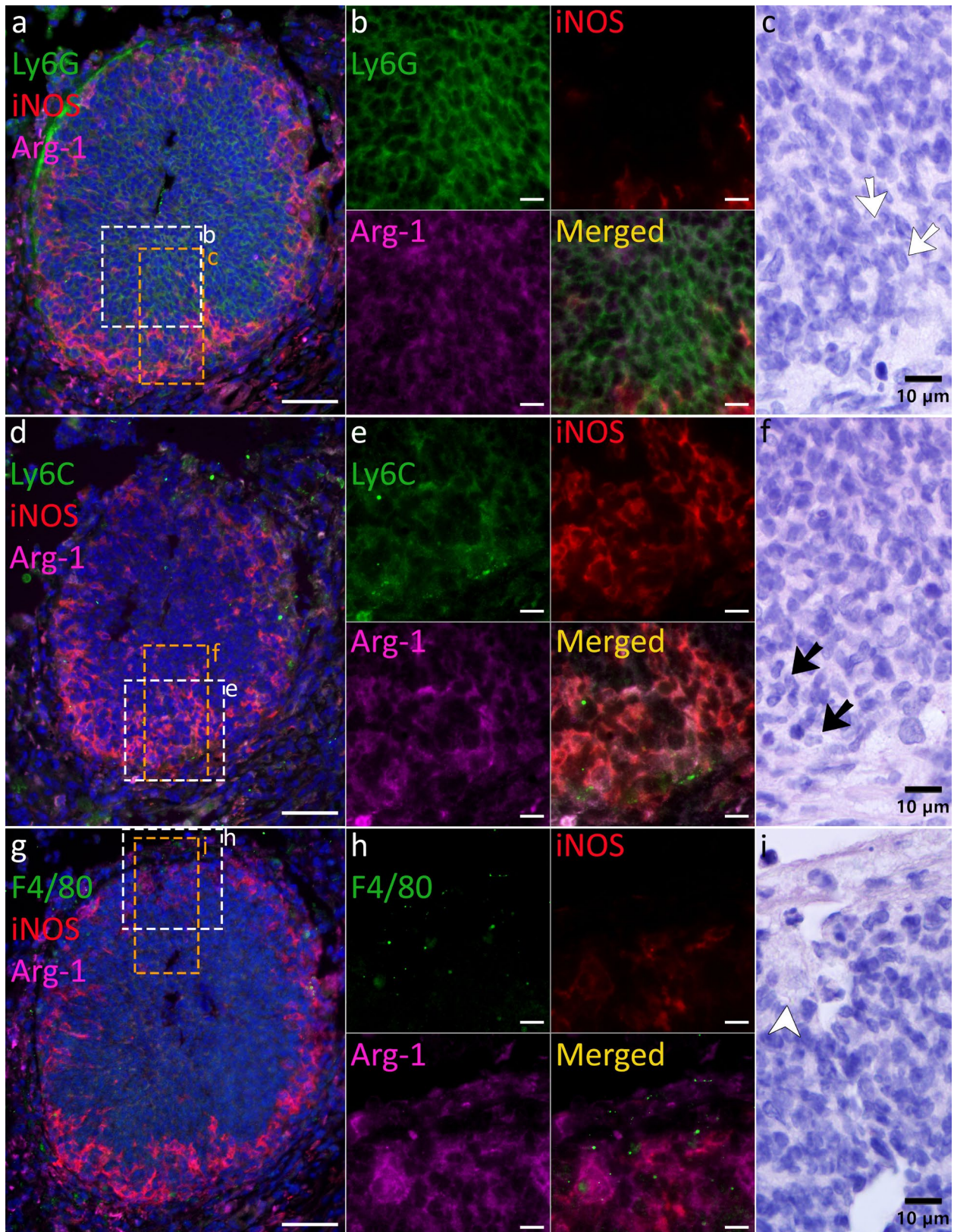


Fig. 5. Innate immune cells within a bone marrow abscess of an *S. aureus*-inoculated murine FRI model 21 d post-surgery. Immunofluorescent staining for (a,b) either Ly6G (neutrophils, green), (d,e) Ly6C (monocytic cells, green) or (h,g) F4/80 (macrophages, green) co-stained with iNOS (enzyme NO production, red) and Arg-1 (enzyme urea cycle, violet) and subsequently stained with (c,f,i) H&E. DAPI (nuclei, dark blue) was used as a counter stain for the fluorescent lower magnification images. In the H&E images, white arrows indicate neutrophils, black arrows show monocytes and a white arrowhead points out a macrophage. Scale bars: (a,d,g) 50 μm and (b,e,h) 10 μm .

or neutrophilic CD11b⁺ Ly6C⁺ Ly6G⁺ cells to detect possible suppressive capabilities. When examining the effects on the total CD3⁺ CD4⁺ T cell fraction, it was observed that monocytic D11b⁺ Ly6C⁺ Ly6G⁻ cells from inoculated mice strongly suppressed T cell proliferation in a ratio-dependent manner, whereas the same cell type from non-inoculated mice did not suppress T cell proliferation (Fig. 6c). Neutrophilic CD11b⁺ Ly6C⁺ Ly6G⁺ cells from non-inoculated mice also did not have suppressive activity towards CD3⁺ CD4⁺ T cells. However, neutrophilic CD11b⁺ Ly6C⁺ Ly6G⁺ cells from inoculated mice significantly suppressed CD3⁺ CD4⁺ T cell proliferation (Fig. 6c). Similar results were observed for CD3⁺ CD8 α ⁺ T cell co-cultured with monocyte or neutrophil fractions from non-inoculated or inoculated mice, although

neutrophilic cells from inoculated mice suppressed CD3⁺ CD8 α ⁺ T cells less than monocytic cells (Fig. 6d).

Discussion

To get a better understanding of the pathophysiology of an FRI, the histopathological changes that occur in an FRI mouse model were examined over time and compared to normal fracture healing processes in non-inoculated mice. The infection in this model progressed into an active, a so-called, chronically florid infection, with constant granulocytes presence, severe osteolysis of the operated femur and many abscesses containing SACs within the bone marrow of the osteotomy segment and adjacent

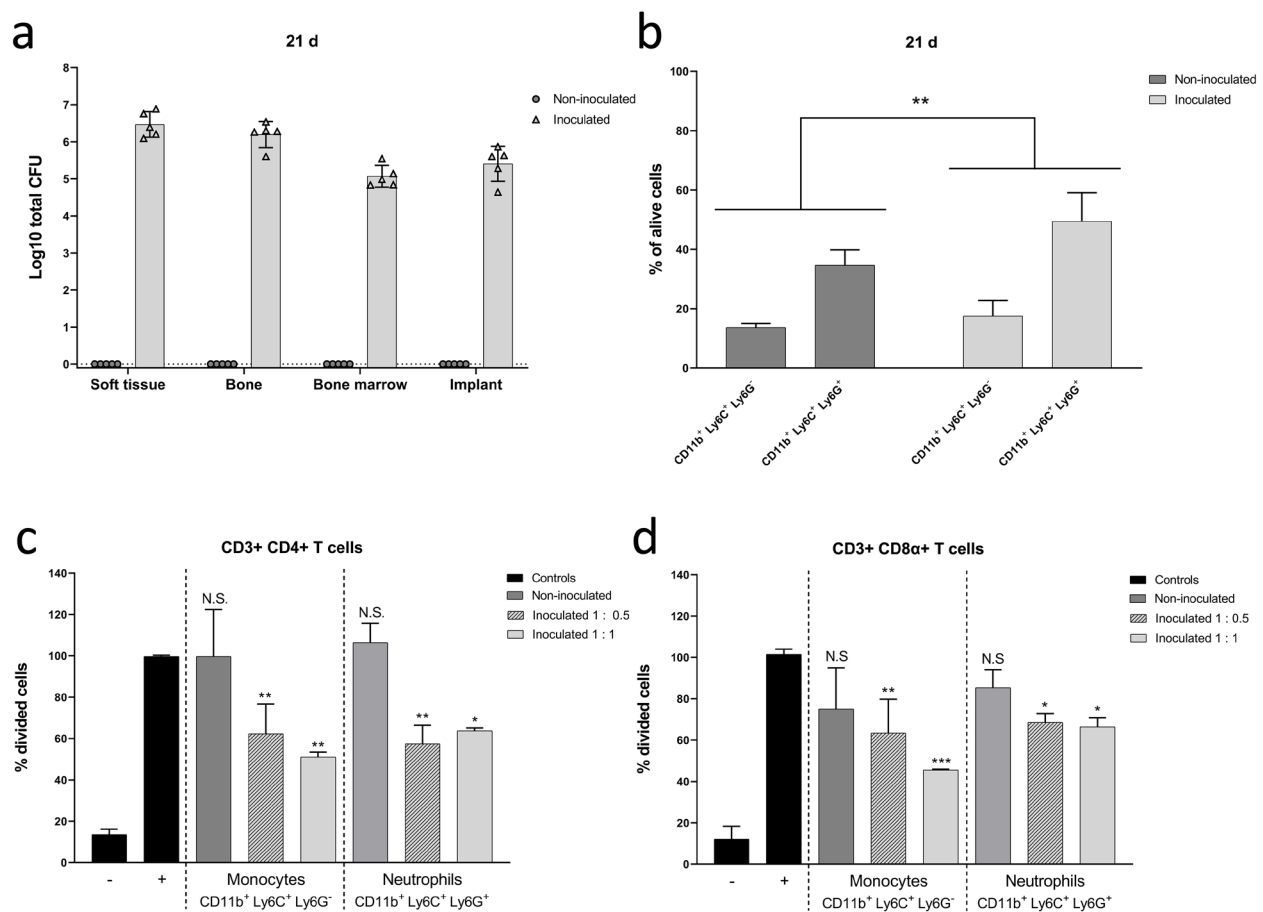


Fig. 6. Evaluation of CFU and monocyte and neutrophil populations in non-inoculated and *S. aureus*-inoculated mice 21 d post-operative. (a) CFU quantification of soft tissues, bones, bone marrow supernatants and implants from non-inoculated (circles) or *S. aureus*-inoculated (triangles) mice used for purification of CD11b⁺ Ly6C⁺ Ly6G⁻ monocytic or CD11b⁺ Ly6C⁺ Ly6G⁺ neutrophilic bone marrow cells 21 d post-surgery. Data are means \pm SD ($n = 5$). (b) Percentage of monocytic CD11b⁺ Ly6C⁺ Ly6G⁻ or neutrophilic CD11b⁺ Ly6C⁺ Ly6G⁺ cells from all alive bone marrow cells of non-inoculated (dark grey) or *S. aureus*-inoculated mice (light grey). Statistical test used: two-way ANOVA comparing cell percentages of inoculated and non-inoculated mice. Data presented are means \pm SD ($n = 5$). Percentage proliferating (c) CD3⁺ CD4⁺ T cells or (d) CD3⁺ CD8 α ⁺ T cells cultured alone without or with CD3/CD28 Dynabeads and rIL2 stimulation (black – or +, respectively) or co-cultures with monocytic CD11b⁺ Ly6C⁺ Ly6G⁻ or neutrophilic CD11b⁺ Ly6C⁺ Ly6G⁺ bone marrow cells from non-inoculated (1 : 1 ratio, dark grey) or *S. aureus*-inoculated mice (1 : 1 ratio, light grey; 0.5 : 1 ratio, striped light grey). Statistical test used: Sidak multiple comparison test. Data are means \pm SD ($n = 5$), stimulated T cells cultured alone were set as 100 % and used as comparison for the statistical tests. N.S.: non-significant, * $p < 0.05$, ** $p < 0.01$, *** $p < 0.001$.

femoral bone. The SACs were covered by a fibrin pseudocapsule surrounded by neutrophils and by an early encapsulation comprised of fibrinogen and collagen. Furthermore, the *S. aureus* infection led to functionally suppressive monocytes and neutrophils and immunohistochemistry revealed the presence of many neutrophils and a few monocytes, anti-inflammatory macrophages (M2) and Tregs.

The most obvious feature of the *S. aureus* infection in the histological sections were the *S. aureus* aggregates, or immature SACs, which were present in the bone marrow of inoculated mice after 3 d. By inoculating the bacteria directly into the bone marrow of the double osteotomy-induced bone segment, a deep osteomyelitis with high chances of SAC formation was preferentially seeded, with relatively less chance for an implant-related biofilm infection. The SACs and abscesses surrounding them evolved into more distinct structures over time. Once matured, the abscesses appeared to be encapsulated by myofibroblasts with collagen and fibrin(ogen) fibres, possibly as an attempt by the host to contain the infection (Kobayashi *et al.*, 2015) and shield it off from neighbouring, healthy tissue. The SACs themselves were surrounded by a fibrin pseudocapsule, which is formed by the action of *S. aureus* within the SAC. *S. aureus* is known to bind fibrin(ogen) using proteins such as ClfA, Emp and Eap (Chavakis *et al.*, 2005; Foster *et al.*, 2014). Furthermore, it has the ability to activate host prothrombin with Coa and vWbp to convert fibrinogen into fibrin (Bjerketorp *et al.*, 2004; Friedrich *et al.*, 2003; Thomer *et al.*, 2016b). Others have suggested that the pseudocapsule around SACs contains fibrin (Cheng *et al.*, 2011; Thomer *et al.*, 2016b), which was confirmed in the present study using a histochemical staining for fibrin. Immunostainings with an anti-fibrin(ogen) antibody did not stain the

pseudocapsule directly around SACs in the present and previous studies (Cheng *et al.*, 2010; Farnsworth *et al.*, 2017). However, the fibrin pseudocapsule did stain positive for fibrin when using the histochemical picro-Mallory trichrome staining (Fig. 3e). The picro-Mallory staining does not depend on antigen binding sites but rather, by combining three different dyes and two staining differentiators, the acid fuchsin stain is retained specifically in the fibrin (Lendrum *et al.*, 1962). The fibrin pseudocapsule of an *in vitro* SAC also is stained in magenta, indicative of fibrin, when the picro-Mallory staining is applied (Hofstee *et al.*, 2020b). Furthermore, *in vitro*, the fibrin pseudocapsule around SACs is stained with an anti-fibrin(ogen) antibody (Hofstee *et al.*, 2020b). These observations strongly suggest that the SAC is surrounded by a fibrin pseudocapsule; however, the precise reason for a lack of specific staining *in vivo* remains unresolved at the present time. Based on the marked accumulation of leukocytes at the edge of the pseudocapsule, it appears that the fibrin pseudocapsule serves to prevent infiltration of immune cells into the SAC and that its formation is one of the key *S. aureus* mechanisms to escape from host responses, as previously suggested (Cheng *et al.*, 2011; Masters *et al.*, 2019; Thomer *et al.*, 2016b). Recently Hofstee *et al.* (2020b) have shown, using an *in vitro* SAC model, that indeed fibrin is abundantly present in the SAC pseudocapsule and this prevents neutrophils from invading a SAC. Moreover, a fibrin pseudocapsule also inhibits the diffusion of antibiotics into the SAC (Hofstee *et al.*, 2020b).

S. aureus aggregation with fibrin or SAC formation may be a target for future FRI therapy and has indeed been shown to be an effective target in, for example, *S. aureus*-related renal infections and endocarditis. Vaccines against Emp and Eap lower abscess numbers

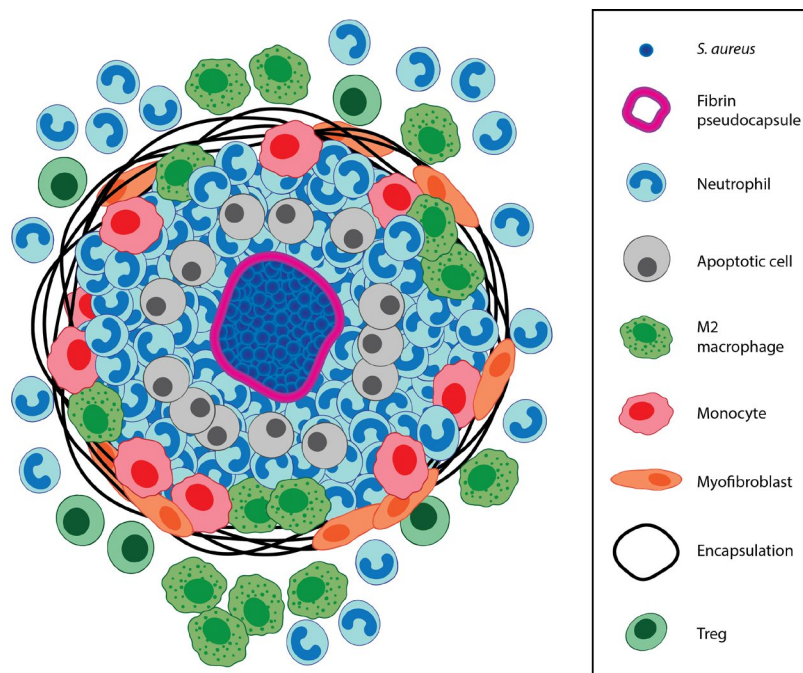


Fig. 7. Schematic overview of the different components of an abscess as observed in a murine FRI model that was partially generated with BioRender (Toronto, ON, Canada).

in a mouse model of renal *S. aureus* infection (Cheng *et al.*, 2009). The anticoagulant dabigatran, which prevents the conversion of fibrinogen into fibrin, decreases the severity of *S. aureus* skin infections and lowers subcutaneous abscess volume (Vanassche *et al.*, 2011). A similar approach may be applied for an FRI but given that fibrin is also important for fracture healing, targeting only bacterial proteins involved in the conversion of fibrinogen into fibrin would be preferred. Such a bacterial protein could be Coa, which when bound to prothrombin forms the enzymatically active staphylothrombin. In a murine *S. aureus* bloodstream infection model, mice are less strongly affected when binding of fibrinogen to Coa was prevented with an antibody against the R-domain of Coa (Thomer *et al.*, 2016a). Other possible options would be to target a conserved domain of vWbp, which when bound to prothrombin can also convert fibrinogen into fibrin, or to target ClfA. ClfA can bind fibrinogen/fibrin and has been associated with *S. aureus* aggregation and mice are less affected by *S. aureus* sepsis when treated with an anti-ClfA antibody (McAdow *et al.*, 2011).

Although others have described most of the neutrophils within an *S. aureus*-related abscess to be dead (Cheng *et al.*, 2011; Thomer *et al.*, 2016b) and, normally, neutrophils are considered to be short-lived (Nicolás-Ávila *et al.*, 2017), it is reasonable to assume that the neutrophils surrounding the SAC in the present mouse model were alive, since they did not stain positive with the TUNEL assay and showed morphological features of live cells. Recent literature supports the observation of neutrophils potentially being long lived under certain conditions, such as certain inflammatory conditions. Moreover, they are now believed to be more diverse in their capabilities, *e.g.* hyper proinflammatory or immunosuppressive, than previously thought (Nicolás-Ávila *et al.*, 2017). Furthermore, microbiota-derived endotoxins and other molecules such as peptidoglycans can influence neutrophil ageing and can prime neutrophil functions to be effective against the infection (Nicolás-Ávila *et al.*, 2017). The bacteria within a SAC might secrete similar factors, which prolong the lifespan of the neutrophils close to the SAC and modulate them to have specific immunomodulatory capabilities; however, this still remains unknown. The TUNEL assay identifies apoptotic cells and possibly also necroptotic cells; in the present study it resulted in a few positive stained cells within the abscess but not bordering the SAC. It would be interesting to examine whether other types of cell death *e.g.* pyroptosis, autophagy or NETosis (Dąbrowska *et al.*, 2019) occur within an abscess to further elucidate the vitality and death of neutrophils associated with abscesses.

14 mice were excluded from further analysis, 12 of which due to a fracture. The mouse model described in the present study is complex and correct placement of the plate and screws is crucial. Consequently, when done inappropriately, there may be mechanical failures in the early post-operative period, unrelated

to infection. At later time points when the infection progressed, there is a risk of screw and implant instability and, thus, fractures due to infection-induced osteolysis.

CD11b⁺ Ly6C⁺ Ly6G⁻ monocytes and CD11b⁺ Ly6C⁺ Ly6G⁺ neutrophils isolated from bone marrow of inoculated mice functionally suppressed T cell proliferation. The suppressive action of these monocytes and neutrophils, together with typical MDSC surface markers, identifies these cells to be monocytic and neutrophilic/granulocytic MDSCs, respectively (Bronte, 2016). MDSCs suppress other immune cells and have previously been associated with chronic *S. aureus* infection. Mice intravenously infected with *S. aureus* have MDSCs in their spleen (Tebartz *et al.*, 2015) and in mice with orthopaedic biofilm infection MDSCs are found in tissue surrounding the implant (Heim *et al.*, 2014). Furthermore, human biopsies from PJI patients collected during joint revision surgeries contain MDSC-like cells (Heim *et al.*, 2015b). The presence of these cells is in line with the development of a persistent infection, since suppressive immune responses will interfere with infection clearance (Heim *et al.*, 2015a).

MDSCs suppress other immune cells by upregulating iNOS and/or Arg-1 and releasing molecules including ROS, IL-10, TGF- β and PGE2 to promote *e.g.* Treg and regulatory B cell induction (Ostrand-Rosenberg and Fenselau, 2018; Veglia *et al.*, 2018). At the border of the abscesses, Ly6C⁺ monocytes simultaneously expressing iNOS and Arg-1 were identified, a feature observed only for monocytic MDSCs (Damuzzo *et al.*, 2015). Interestingly, to the best of the authors' knowledge, monocytes being part of an abscess have not been described to date. Furthermore, the Ly6G⁺ neutrophils around the SAC expressed Arg-1, not a characteristic of neutrophils per se, but certainly of granulocytic MDSCs (Veglia *et al.*, 2018). Cells positive for Arg-1 protein are present close to SACs, as determined by spatially targeted proteomics (Guiberson *et al.*, 2020). Possibly, the neutrophils around the SAC and within the abscess and the monocytes at the outer rim of the abscess are MDSCs and have suppressive capabilities through Arg-1 or both Arg-1 and iNOS, respectively. This would explain the presence of FOXP3⁺ Tregs and M2 macrophages around the abscess. More *ex vivo/in vitro* investigations are required to assess specifically the immunosuppressive capabilities of these cells. Additionally, it may be that the neutrophils and monocytes together with the M2 macrophages within the abscess initiate encapsulation by secreting high levels of TGF- β , a pro-fibrotic factor, which upregulates genes involved in extracellular matrix production by fibroblasts and myofibroblasts (Leask and Abraham, 2004). This would also be an interesting future direction of research.

To lower bacterial burden and prevent persistent infection in an FRI, an option would be to target the MDSCs by using an antibody therapy against

Ly6G, as performed in a murine femoral *S. aureus* orthopaedic biofilm infection model (Heim *et al.*, 2014). This therapy decreases granulocytic MDSC levels and subsequently decreases bacterial loads in tissue surrounding the implant and the knee joint (Heim *et al.*, 2014). Local application of anti-MDSC therapy may be key for this treatment approach (Tebartz *et al.*, 2015).

Normally, and indeed observed in the non-inoculated mice (data not shown), a shift from proinflammatory M1 towards anti-inflammatory M2 macrophages occurs during fracture healing. The first 3 d after fracture M1 macrophages predominate, whereas by 7 d M2 macrophages prevail (Schlundt *et al.*, 2018; Wasnik *et al.*, 2018). However, in the present study, inoculated animals had minimal numbers of M1 macrophages and mostly M2 macrophages after 7 d. *S. aureus* biofilm can skew macrophages to an M2 phenotype *in vivo* (Thurlow *et al.*, 2011). This might happen because TLR ligands on *S. aureus* are not accessible for macrophages when *S. aureus* is within a biofilm (Thurlow *et al.*, 2011). A similar process may occur for SACs, which are effectively sealed off from host cells by the fibrin pseudocapsule. When preventing *S. aureus* from growing in a fibrin pseudocapsule by one of the treatment strategies mentioned above, TLR ligands might be more exposed and macrophages might stay in a proinflammatory state instead of being skewed towards an anti-inflammatory state. Another interesting treatment option for an FRI is metabolically reprogramming monocytes/macrophages to become proinflammatory with oligomycin nanoparticles, as was shown in a mouse model of *S. aureus* PJI (Yamada *et al.*, 2020). In addition to changing the metabolic state of monocytes, this therapy also indirectly changed the metabolic state of MDSCs (Yamada *et al.*, 2020).

Taken together, in an *S. aureus* FRI, abscesses contained a central *S. aureus* SAC within a fibrin pseudocapsule. The SAC was surrounded by live neutrophils with only few apoptotic cells, with a mixture of monocytes and M2 macrophages at the border of an abscess. The abscess encapsulation consists of α SMA⁺ myofibroblast, collagen and fibrinogen. Around the abscess, neutrophils, M2 macrophages and Tregs were observed (Fig. 7). The resulting condition in the tissue likely was anti-inflammatory and causally related to the persistent *S. aureus* infection.

Conclusions

The study provided an in-depth description of the histopathology of an *S. aureus* FRI as it progressed over time. Fibrin-covered SACs were present within bone marrow abscesses and these abscesses were themselves encapsulated by collagen, fibrinogen and myofibroblasts. Outside the SAC, and inside the abscess margins, the dense accumulation of cells,

primarily neutrophils and a few monocytes, were largely vital and showed immunohistochemical markers consistent with granulocytic or monocytic MDSCs, respectively. The bone marrow also contained functionally immunosuppressive MDSCs, M2 macrophages and Tregs, further indicating the local environment to be anti-inflammatory. By better understanding the local inflammatory conditions that lead to the persistence of an infection and the physical features of SACs, it may enable tailored treatment regimens for FRIs.

Acknowledgements

The authors would like to thank the preclinical facility of the AO Research Institute Davos, Iris Keller, Dr Eamon Sheehy, Jolien Onsea, Aron Keshishian and Susanne Bärtil for their contribution to the animal studies. For help with the (immuno) stains, bone marrow cell and splenocyte isolation as well as imaging, the authors would like to thank Pamela Furlong. Additionally, the authors would like to thank the Innovationsstiftung Graubünden for kindly donating the FACSaria III and Dr Ursula Menzel for her help with sorting the bone marrow cells. This work was supported by AOTrauma grant AR2017_05 as part of the Clinical Priority Program on Bone Infection.

References

- Alt V, Lips KS, Henkenbehrens C, Muhrer D, Oliveira Cavalcanti MC, Sommer U, Thormann U, Szalay G, Heiss C, Pavlidis T, Domann E, Schnettler R (2011) A new animal model for implant-related infected non-unions after intramedullary fixation of the tibia in rats with fluorescent *in situ* hybridization of bacteria in bone infection. *Bone* **48**: 1146-1153.
- Bezstarosti H, Van Lieshout EMM, Voskamp LW, Kortram K, Obremskey W, McNally MA, Metsemakers WJ, Verhofstad MHJ (2019) Insights into treatment and outcome of fracture-related infection: a systematic literature review. *Arch Orthop Trauma Surg* **139**: 61-72.
- Bjerketorp J, Jacobsson K, Frykberg L (2004) The von Willebrand factor-binding protein (vWbp) of *Staphylococcus aureus* is a coagulase. *FEMS Microbiol Lett* **234**: 309-314.
- Bose D, Kugan R, Stubbs D, McNally M (2015) Management of infected nonunion of the long bones by a multidisciplinary team. *Bone Joint J* **97-b**: 814-817.
- Brandt SL, Putnam NE, Cassat JE, Serezani CH (2018) Innate immunity to *Staphylococcus aureus*: evolving paradigms in soft tissue and invasive infections. *J Immunol* **200**: 3871-3880.
- Bronte V, Brandau S, Chen SH, Colombo MP, Frey AB, Greten TF, Mandruzzato S, Murray PJ, Ochoa

- A, Ostrand-Rosenberg S, Rodriguez PC, Sica A, Umansky V, Vonderheide RH, Gabrilovich DI (2016) Recommendations for myeloid-derived suppressor cell nomenclature and characterization standards. *Nat Commun* **7**: 12150. DOI: 10.1038/ncomms12150.
- Brown JH, Brenn LA (1931) A method for the differential staining of Gram positive and Gram negative bacteria in tissue sections. *Bulletin of the John Hopkins* **XLVIII**: 69-73.
- Chavakis T, Wiechmann K, Preissner KT, Herrmann M (2005) *Staphylococcus aureus* interactions with the endothelium: the role of bacterial "secretable expanded repertoire adhesive molecules" (SERAM) in disturbing host defense systems. *Thromb Haemost* **94**: 278-285.
- Cheng AG, DeDent AC, Schneewind O, Missiakas D (2011) A play in four acts: *Staphylococcus aureus* abscess formation. *Trends Microbiol* **19**: 225-232.
- Cheng AG, Kim HK, Burts ML, Krausz T, Schneewind O, Missiakas DM (2009) Genetic requirements for *Staphylococcus aureus* abscess formation and persistence in host tissues. *FASEB J* **23**: 3393-3404.
- Cheng AG, McAdow M, Kim HK, Bae T, Missiakas DM, Schneewind O (2010) Contribution of coagulases towards *Staphylococcus aureus* disease and protective immunity. *PLoS Pathog* **6**: e1001036. DOI: 10.1371/journal.ppat.1001036.
- Dąbrowska D, Jabłońska E, Iwaniuk A, Garley M (2019) Many ways-one destination: different types of neutrophils death. *Int Rev Immunol* **38**: 18-32.
- Damuzzo V, Pinton L, Desantis G, Solito S, Marigo I, Bronte V, Mandruzzato S (2015) Complexity and challenges in defining myeloid-derived suppressor cells. *Cytometry B Clin Cytom* **88**: 77-91.
- Farnsworth CW, Schott EM, Jensen SE, Zukoski J, Benvie AM, Refaai MA, Kates SL, Schwarz EM, Zuscik MJ, Gill SR, Mooney RA (2017) Adaptive upregulation of clumping factor A (ClfA) by *Staphylococcus aureus* in the obese, type 2 diabetic host mediates increased virulence. *Infect Immun* **85**: e01005-16. DOI: 10.1128/IAI.01005-16.
- Foster TJ, Geoghegan JA, Ganesh VK, Hook M (2014) Adhesion, invasion and evasion: the many functions of the surface proteins of *Staphylococcus aureus*. *Nat Rev Microbiol* **12**: 49-62.
- Friedrich R, Panizzi P, Fuentes-Prior P, Richter K, Verhamme I, Anderson PJ, Kawabata S, Huber R, Bode W, Bock PE (2003) Staphylocoagulase is a prototype for the mechanism of cofactor-induced zymogen activation. *Nature* **425**: 535-539.
- Guiberson ER, Weiss A, Ryan DJ, Monteith AJ, Sharman K, Gutierrez DB, Perry WJ, Caprioli RM, Skaar EP, Spraggins JM (2020) Spatially targeted proteomics of the host-pathogen interface during staphylococcal abscess formation. *ACS Infect Dis* **7**: 101-113.
- Heim CE, Vidlak D, Kielian T (2015a) Interleukin-10 production by myeloid-derived suppressor cells contributes to bacterial persistence during *Staphylococcus aureus* orthopedic biofilm infection. *J Leukoc Biol* **98**: 1003-1013.
- Heim CE, Vidlak D, Odvody J, Hartman CW, Garvin KL, Kielian T (2018) Human prosthetic joint infections are associated with myeloid-derived suppressor cells (MDSCs): implications for infection persistence. *J Orthop Res* **36**: 1605-1613.
- Heim CE, Vidlak D, Scherr TD, Hartman CW, Garvin KL, Kielian T (2015b) IL-12 promotes myeloid-derived suppressor cell recruitment and bacterial persistence during *Staphylococcus aureus* orthopedic implant infection. *J Immunol* **194**: 3861-3872.
- Heim CE, Vidlak D, Scherr TD, Kozel JA, Holzapfel M, Muirhead DE, Kielian T (2014) Myeloid-derived suppressor cells contribute to *Staphylococcus aureus* orthopedic biofilm infection. *J Immunol* **192**: 3778-3792.
- Hofstee MI, Muthukrishnan G, Atkins GJ, Riool M, Thompson K, Morgenstern M, Stoddart MJ, Richards RG, Zaat SAJ, Moriarty TF (2020a) Current concepts of osteomyelitis: from pathologic mechanisms to advanced research methods. *Am J Pathol* **190**: 1151-1163.
- Hofstee MI, Riool M, Terjajevs I, Thompson K, Stoddart MJ, Richards RG, Zaat SAJ, Moriarty TF (2020b) Three-dimensional *in vitro* *Staphylococcus aureus* abscess communities display antibiotic tolerance and protection from neutrophil clearance. *Infect Immun* **88**: e00293-20. DOI: 10.1128/IAI.00293-20.
- Huh J, Stinner DJ, Burns TC, Hsu JR (2011) Infectious complications and soft tissue injury contribute to late amputation after severe lower extremity trauma. *J Trauma* **71**: S47-51.
- Kanakaris N, Gudipati S, Tosounidis T, Harwood P, Britten S, Giannoudis PV (2014) The treatment of intramedullary osteomyelitis of the femur and tibia using the reamer-irrigator-aspirator system and antibiotic cement rods. *Bone Joint J* **96-b**: 783-788.
- Klosterhalfen B, Peters KM, Tons C, Hauptmann S, Klein CL, Kirkpatrick CJ (1996) Local and systemic inflammatory mediator release in patients with acute and chronic posttraumatic osteomyelitis. *J Trauma* **40**: 372-378.
- Kobayashi SD, Malachowa N, DeLeo FR (2015) Pathogenesis of *Staphylococcus aureus* abscesses. *Am J Pathol* **185**: 1518-1527.
- Leask A, Abraham DJ (2004) TGF-beta signaling and the fibrotic response. *Faseb j* **18**: 816-827.
- Lendrum AC, Fraser DS, Slidders W, Henderson R (1962) Studies on the character and staining of fibrin. *J Clin Pathol* **15**: 401-413.
- Masters EA, Trombetta RP, de Mesy Bentley KL, Boyce BF, Gill AL, Gill SR, Nishitani K, Ishikawa M, Morita Y, Ito H, Bello-Irizarry SN, Ninomiya M, Brodell JD Jr, Lee CC, Hao SP, Oh I, Xie C, Awad HA, Daiss JL, Owen JR, Kates SL, Schwarz EM, Muthukrishnan G (2019) Evolving concepts in bone infection: redefining "biofilm", "acute vs. chronic osteomyelitis", "the immune proteome" and "local

antibiotic therapy". *Bone Res* **7**: 20. DOI: 10.1038/s41413-019-0061-z.

McAdow M, Kim HK, Dedent AC, Hendrickx AP, Schneewind O, Missiakas DM (2011) Preventing staphylococcus aureus sepsis through the inhibition of its agglutination in blood. *PLoS Pathog* **7**: e1002307. DOI: 10.1371/journal.ppat.1002307.

Metsemakers WJ, Kuehl R, Moriarty TF, Richards RG, Verhofstad MHJ, Borens O, Kates S, Morgenstern M (2016) Infection after fracture fixation: current surgical and microbiological concepts. *Injury* **49**: 511-522.

Morgenstern M, Kuehl R, Zalavras CG, McNally M, Zimmerli W, Burch MA, Vandendriessche T, Obremskey WT, Verhofstad MHJ, Metsemakers WJ (2021) The influence of duration of infection on outcome of debridement and implant retention in fracture-related infection. *Bone Joint J* **103-b**: 213-221.

Moriarty TF, Campoccia D, Nees SK, Boure LP, Richards RG (2010) *In vivo* evaluation of the effect of intramedullary nail microtopography on the development of local infection in rabbits. *Int J Artif Organs* **33**: 667-675.

Nicolás-Ávila J, Adrover JM, Hidalgo A (2017) Neutrophils in homeostasis, immunity, and cancer. *immunity* **46**: 15-28.

Ochsner PE, Hailemariam S (2006) Histology of osteosynthesis associated bone infection. *Injury* **37**: S49-58.

Ostrand-Rosenberg S, Fenselau C (2018) Myeloid-derived suppressor cells: immune-suppressive cells that impair antitumor immunity and are sculpted by their environment. *J Immunol* **200**: 422-431.

Peng KT, Hsieh CC, Huang TY, Chen PC, Shih HN, Lee MS, Chang PJ (2017) *Staphylococcus aureus* biofilm elicits the expansion, activation and polarization of myeloid-derived suppressor cells *in vivo* and *in vitro*. *PLoS One* **12**: e0183271. DOI: 10.1371/journal.pone.0183271.

Rauch S, DeDent AC, Kim HK, Bubeck Wardenburg J, Missiakas DM, Schneewind O (2012) Abscess formation and alpha-hemolysin induced toxicity in a mouse model of *Staphylococcus aureus* peritoneal infection. *Infect Immun* **80**: 3721-3732.

Schlundt C, El Khassawna T, Serra A, Dienelt A, Wendler S, Schell H, van Rooijen N, Radbruch A, Lucius R, Hartmann S, Duda GN, Schmidt-Bleek K (2018) Macrophages in bone fracture healing: their essential role in endochondral ossification. *Bone* **106**: 78-89.

Tebartz C, Horst SA, Sparwasser T, Huehn J, Beineke A, Peters G, Medina E (2015) A major role for myeloid-derived suppressor cells and a minor role for regulatory T cells in immunosuppression during *Staphylococcus aureus* infection. *J Immunol* **194**: 1100-1111.

Thomer L, Emolo C, Thammavongsa V, Kim HK, McAdow ME, Yu W, Kieffer M, Schneewind O, Missiakas D (2016a) Antibodies against a secreted product of *Staphylococcus aureus* trigger phagocytic killing. *J Exp Med* **213**: 293-301.

Thomer L, Schneewind O, Missiakas D (2016b) Pathogenesis of *Staphylococcus aureus* bloodstream infections. *Annu Rev Pathol* **11**: 343-364.

Thurlow LR, Hanke ML, Fritz T, Angle A, Aldrich A, Williams SH, Engebretsen IL, Bayles KW, Horswill AR, Kielian T (2011) *Staphylococcus aureus* biofilms prevent macrophage phagocytosis and attenuate inflammation *in vivo*. *J Immunol* **186**: 6585-6596.

Tiemann A, Hofmann GO, Krukemeyer MG, Krenn V, Langwald S (2014) Histopathological osteomyelitis evaluation score (HOES) - an innovative approach to histopathological diagnostics and scoring of osteomyelitis. *GMS Interdiscip Plast Reconstr Surg DGPW* **3**: Doc08. DOI: 10.3205/iprs000049.

Trampuz A, Zimmerli W (2006) Diagnosis and treatment of infections associated with fracture-fixation devices. *Injury* **37 Suppl 2**: S59-66.

Vanassche T, Verhaegen J, Peetermans WE, J VANR, Cheng A, Schneewind O, Hoylaerts MF, Verhamme P (2011) Inhibition of staphylothrombin by dabigatran reduces *Staphylococcus aureus* virulence. *J Thromb Haemost* **9**: 2436-2446.

Veglia F, Perego M, Gabrilovich D (2018) Myeloid-derived suppressor cells coming of age. *Nat Immunol* **19**: 108-119.

Wasnik S, Rundle CH, Baylink DJ, Yazdi MS, Carreon EE, Xu Y, Qin X, Lau KW, Tang X (2018) 1,25-Dihydroxyvitamin D suppresses M1 macrophages and promotes M2 differentiation at bone injury sites. *JCI Insight* **3**: e98773. DOI: 10.1172/jci.insight.98773.

Yamada KJ, Heim CE, Xi X, Attri KS, Wang D, Zhang W, Singh PK, Bronich TK, Kielian T (2020) Monocyte metabolic reprogramming promotes pro-inflammatory activity and *Staphylococcus aureus* biofilm clearance. *PLoS Pathog* **16**: e1008354. DOI: 10.1371/journal.ppat.1008354.

Discussion with Reviewers

Robert Mooney: Having concluded that the present mouse FRI model reflected an acute infection, how might the model be modified to represent a chronic infection?

Authors: The mouse FRI model used indeed did not represent a chronic infection but mice had an initial acute infection that progressed to a chronically florid/active infection after 28 d. *S. aureus* predominantly causes relatively acute infections in human patients and chronic infections are more common with coagulase-negative staphylococci. Nevertheless, chronic *S. aureus* infections do occur, for example after failed revisions or suppressive long term antibiotic therapy. The reason that the present mouse FRI model did not represent a chronic infection might be due to a time-related issue. An indication for this is that the encapsulation around the abscesses was still relatively immature at 28 d. If later time points were chosen, the entire abscess structure might have developed and become more mature.

By this time, there may also be more lymphocyte and macrophage infiltration, characteristic of a chronic infection rather than a neutrophil infiltration. However, it is important to note that there is a risk that longer observation periods would likely lead to continued osteolysis, leading eventually to a failure of the implant and the need to exclude the animal. Increased implant failure rates have been observed in past studies as the observation period increases. Thus, this infection model may be more suited to study effects at earlier timepoints. One possibility to allow for extended observation periods may be to administer a low dose of suppressive antibiotics, to maintain the infection in a relatively controlled state and to allow the encapsulation to mature and the host defences to organise. However, at the present time, it is unknown how such antibiotic therapy may change the course of the infection, but this would be the most appropriate means to begin developing a chronic infection model.

Reviewer: In the discussion, the authors state the following: "A similar approach may be applied for an FRI but given that fibrin is also important for fracture healing, targeting only bacterial proteins involved in the conversion of fibrinogen into fibrin would be preferred". The authors only briefly discussed a very important issue. Targeting fibrin would negatively influence fracture healing. Do the authors have other targets in mind?

Authors: Yes, we indeed do have other targets in mind. Instead of targeting the conversion of fibrinogen into

fibrin with a generic thrombin inhibitor that inhibits both the host thrombin as well as staphylothrombin, a more desired approach would be to target staphylothrombin specifically. Staphylothrombin is a combination of either Coa or vWbp with the host prothrombin, making the proenzyme active. Thomer *et al.* (2016a) have shown that the highly conserved R-domain of Coa can be targeted with an antibody causing less fibrin-mediated aggregation of *S. aureus* and a drop in *S. aureus* infection rates. A similar approach might be used for vWbp. Besides inhibiting the conversion of fibrinogen into fibrin by *S. aureus* proteins, an option would be to block *S. aureus* binding to fibrinogen/fibrin by for example using an anti-ClfA antibody or to block both the binding of fibrinogen/fibrin and staphylothrombin. When *S. aureus* is not able to aggregate and surround itself with fibrin, immune cells may have a chance in clearing the bacteria, which might subsequently prevent the expansion of immunosuppressive MDSCs and anti-inflammatory macrophages. Furthermore, an option would be to directly prevent the expansion of immunosuppressive MDSCs and anti-inflammatory macrophages by, for example, using a local antibody therapy against MDSCs or by metabolically reprogramming monocytes/macrophages to become proinflammatory with oligomycin nanoparticles, respectively.

Editor's note: The Guest Editor responsible for this paper was Henny Van der Mei.